ADVANCED MATERIALS

# Structural Characterization of Non-Oxide Chalcogenide Glasses using Solid State NMR **

Magic Angle Spinning
Internal Interactions
Selective Averaging
B/Si/P Based Glasses
Infrared Optics
Semiconductor Technology

By Hellmut Eckert *

*Dedicated to Prof. W. Müller-Warmuth on the occasion of his 60th birthday*

**In spite of the long-standing importance of non-oxide chalcogenide glasses in infrared optics and semiconductor technology, concepts describing the structural principles governing glass formation in these systems are just emerging. Most recently, modern quantitative solid state NMR techniques have offered new unique insights into the structural organization of these systems. In this review, we discuss the basic principles of various experimental approaches and their application to boron- silicon,- and phosphorus chalcogenide glasses.**

## 1. Introduction

Non-oxide chalcogenide glasses, which are based on the sulfides, selenides, and tellurides of the main group III–V elements, have recently gained much interest as materials for infrared-transparent optical fibers,[1] reversible conductivity switching devices,[2] semiconductors,[3] photoconductors, photoresists,[4] and solid electrolytes for battery applications.[5] Generally, glasses are often preferred over crystalline compounds because of their favorable mechanical and interfacing characteristics, and because their materials properties can be tailored for specific applications by continuously varying their composition or processing conditions. In the area of non-oxide chalcogenide glasses, however, substantial challenges have remained due to the air- and moisture sensitivity and the low glass transition temperatures of many systems.

Figure 1 shows the most common constituent elements of such glasses. During the last two decades, much work has been devoted to the phase diagrams, regions of glass-formation, and the thermodynamic and physicochemical properties of these systems.[6] It has been much more recently that, driven by the search for structural guidelines to optimize materials properties, the microstructure of these glasses has moved into the focus of attention. At the same time (and for similar reasons) chalcogenide glasses have become an increasingly attractive subject for theoreticians and solid-state physicists.[7–10]

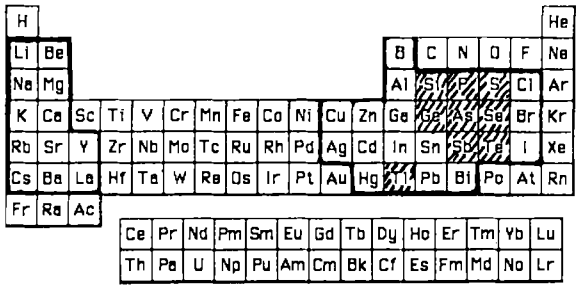


Fig. 1. Elements that participate in the formation of covalent non-oxidic glasses. Dashed lines indicates those elements that occur most commonly in such glasses.

According to most recent spectroscopic studies, the structure of chalcogenide glasses is characterized by several unique features not commonly found in other types of glasses. These features include: a) valence alternation pairs, b) new types of micro-environments not known in analogous crystalline compounds, and c) clusters or polymeric entities with a high degree of intermediate-range order. Figure 2 shows a few recent examples from the literature.

While these novel findings represent substantial progress, they mark only the beginning of a qualitative and quantitative understanding of chalcogenide glasses. The identification and quantification of specific structural features has often remained controversial, since most of the spectroscopic techniques used are not inherently quantitative and tend to emphasize ordered environments. Moreover, the proposals made for individual systems are conceptually somewhat divergent, which reflects a current inability to explain the

[*] Prof. H. Eckert
Department of Chemistry, University of California, Santa Barbara, Goleta, CA 93106 (USA)

[**] The author is very grateful to his scientific mentor, Prof. *W. Müller-Warmuth*, who, a decade ago, introduced him to solid state NMR theory and techniques. Thanks are due to my coworkers at UC Santa Barbara, *M. Drake, D. Lathrop, T. Luong, K. Moran, M. Tullius*, and *Zh. Zhang*, and my collaborators *Dr. J. H. Kennedy* and Dr. *M. Ribes* for their many contributions and stimulating discussions. Acknowledgment is made to the Donors of the Petroleum Research Fund administered by the American Chemical Society for partial support of this research. Financial support by the UCSB Academic Senate is also gratefully acknowledged.

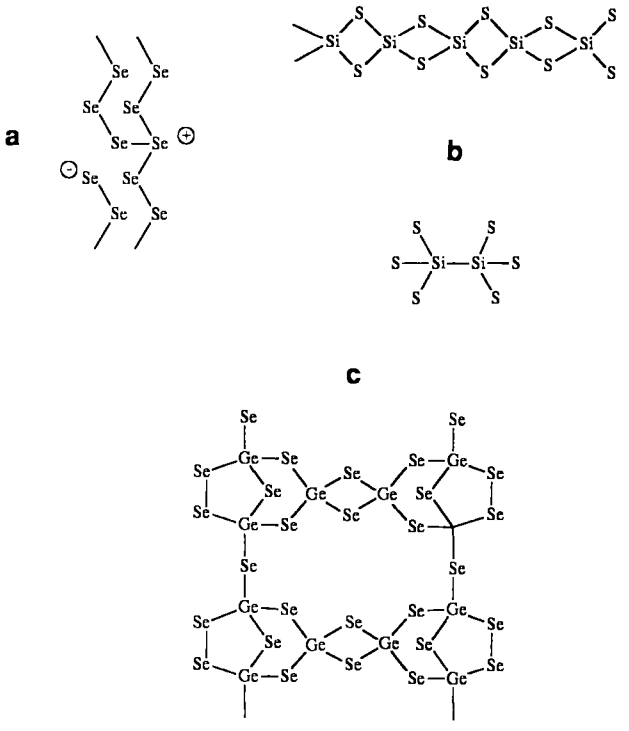


Fig. 2. Unique structural features postulated to occur in non-oxide chalcogenide glasses. a) valence alternation pairs in amorphous selenium [7]. b) edge-shared polymers and ethane-like units in Si–S glasses [8]. c) intermediate-range ordered cluster units in glassy $GeSe_2$ [9].

principles of non-oxide glass formation in more quantitative terms. There is a definite need for new experimental probes that can test the existing structural hypotheses in a more stringent manner than presently possible. Solid state NMR is an element-selective, inherently quantitative method ideally suited for this objective.[11] Since NMR is also spatially very selective, the spectroscopic information remains largely unaffected by the lack of periodicity in non-crystalline systems.

During 25 years of intense research, solid state NMR has proven very useful in developing structural concepts for oxide-based (silicate, borate, and phosphate) glasses.[12] In contrast, the unique power of this technique to provide structural information in chalcogenide systems is just emerging.

## 2. Information Content of Solid State NMR Spectra in Glasses

### 2.1. Fundamental Principles of the Technique

All nuclei containing an odd number of either protons or neutrons or both, possess angular momentum ("spin") and consequently, a magnetic moment. In the presence of an applied magnetic field $B_0$ (typical strength 1–14 T), these nuclei occupy quantized energy levels which are energetically non-degenerate and thus not equally populated. These population differences result in a macroscopic nuclear magnetization along the direction of $B_0$.

NMR spectroscopy measures the precise energy differences between such nuclear levels; this is done by stimulating transitions between them through the application of electromagnetic waves in the radio frequency region (1–600 MHz). At resonance, the condition

$$\omega = \gamma B_{loc} \tag{1}$$

holds, where $\omega$ is the frequency of the electromagnetic radiation at which absorption occurs, $\gamma$ is a nuclear constant, and $B_{loc}$ is the strength of the magnetic field present at the nuclear sites. Usually, a short (1–10 μs length), intense (100–1000 W power) radiofrequency pulse is applied by the spectrometer that tips the magnetization into the plane perpendicular to the magnetic field direction ("90° pulse"). The precession of the magnetization in this plane then induces an ac voltage in a coil, which is amplified, detected, and stored in a computer. Fourier analysis of the acquired "free induction decay signal" then yields $\omega$, the nuclear magnetic resonance frequency.

Signal averaging by repetitive pulsing is usually necessary. For truly quantitative information it is mandatory to allow for sufficient time between pulses to restore the magnetization along $B_0$ to its equilibrium value. The waiting time required depends on the relaxation time $T_1$ of the nuclei, which can range from a few ms to several hours in glasses.

### 2.2. Internal Interactions

The usefulness of NMR in addressing structural questions in matter stems from the fact that the magnitude of $B_{loc}$ (and

*Hellmut Eckert received his PhD in Physical Chemistry at the Westfälische Wilhelms Universität Münster, FRG, in 1982. After two postdoctoral years at Rutgers University, New Brunswick, New Jersey, he held a position as a staff Scientist at the Southern California Regional NMR Facility at the California Institute of Technology, from 1984–1987. Since July 1987, he has been an Assistant Professor of Chemistry at the University of California, Santa Barbara. Prof. Eckert's research is concerned with the synthesis of novel types of non-oxidic glasses and with the development of modern solid state NMR strategies for the structural analysis of disordered materials.*

ADVANCED MATERIALS

hence the nuclear resonance frequency) is usually slightly different from $B_0$, due to various types of internal interactions: The *magnetic dipole-dipole interaction* describes the effect nearby magnetic moments from other atoms have on the local field of the nuclei under observation. The *chemical shift interaction* describes how the local field is modified by the electron clouds surrounding the nuclei, and finally, the *nuclear electric quadrupole coupling* describes the interaction of the asymmetric charge distribution in spin $> \frac{1}{2}$ nuclei with electrostatic field gradients generated by the chemical bonding environment. Each of these interactions is characterized by a few spectroscopic parameters, listed in Table 1.

Table 1. Interactions in solid state NMR, spectroscopic parameters and their selective measurement.

| Interaction | Spectroscopic parameters | Selective measurement | Ref. |
|---|---|---|---|
| dipole-dipole | $M_{2hom.}$ (like nuclei) | 90°–$t_1$–180° echo decay | 14 |
| | $M_{2het.}$ (unlike nuclei) | 90°$_x$–$t_1$–90°$_y$ echo decay | 15 |
| chemical shift | isotropic part, $\delta_{iso}$ | MAS-centerline position | 13 |
| | anisotropic part | MAS sideband intensities | 17 |
| quadrupole | coupling constant ($e^2qQ/h$) | MAS lineshape analysis, 2-D nutation NMR | 16, 16 |
| | asym. parameter $\eta$ | variable angle spinning | 18 |

Mathematically, a tensorial description is used to appropriately reflect the fact that all of these interactions are anisotropic.[11] Consequently, the energy level perturbations (and hence the resonance conditions) depend on the orientation of the crystal (or molecule) with respect to the external magnetic field. Therefore, the spectrum observed in a powder or glass (the "NMR powder pattern") forms the envelope of all resonance conditions arising from all possible orientations.

If one of the three interactions discussed above is much larger than the other ones, the corresponding spectroscopic parameters are usually easily determined from such a powder pattern. However, frequently the various terms are of comparable magnitude, making the spectra difficult to analyze. The situation is complicated further in glasses, where the spectroscopic parameters would be more accurately represented in the form of distribution functions rather than unique values.

The NMR problem thus falls into two sub-tasks: a) accurate parametrization of the experimental spectra and b) correlating the spectroscopic parameters thus obtained with the desired structural information.

### 2.3. Selective Averaging Experiments

The first task is often approached by modifying the relative magnitudes of different interactions in a predictable fashion. Traditionally, this has been done by exploiting field dependence, isotopic dilution, or different isotopes of the same element. Alternatively, elegant selective averaging techniques that suppress certain interactions while leaving others unaffected are being increasingly utilized. Table 1 contains some of the approaches which are most generally applicable.[13–18] In the following, we will discuss briefly two of these techniques, which are of particular interest for the material covered in this review.

The first, most popular, selective averaging experiment uses mechanical sample rotation about an axis inclined by an angle $\beta$ with respect to the external magnetic field direction.[13] This manipulation modulates the anisotropic part of the interaction by the term $(3\cos^2\beta - 1)$. At an angle of 54.7° the orientational dependence of the spectra is removed and a sharp, "liquid-like" resonance is observed at the isotropic chemical shift position. Solid state NMR spectra acquired with this technique are referred to as "MAS" (magic angle spinning) spectra. The isotropic chemical shift $\delta_{iso}$, which is usually quoted in ppm with respect to a chosen reference standard (tetramethyl silane for $^{29}$Si, 85% phosphoric acid for $^{31}$P NMR), is the single most significant NMR observable for compound identification.

The second experiment involves the selective measurement of magnetic dipole-dipole couplings.[14, 15] The magnitude of the dipolar coupling is most commonly expressed in terms of the second moment $M_2$, the average squared local field present at the nuclei due to these interactions. This particular description in terms of a statistical quantity has the advantage that the details of the spin system (numbers and relative geometries of the interacting nuclei involved) need not be known for the analysis, and that homonuclear interactions (between like spins) and heteronuclear interactions (between unlike spins) can be separated.[19] The homonuclear part of $M_2$ can be measured selectively by spin-echo spectroscopy. Figure 3 illustrates the concept. In general, the free induction decay following a 90° radio frequency pulse on resonance can be refocused by a subsequent 180° pulse, resulting in a

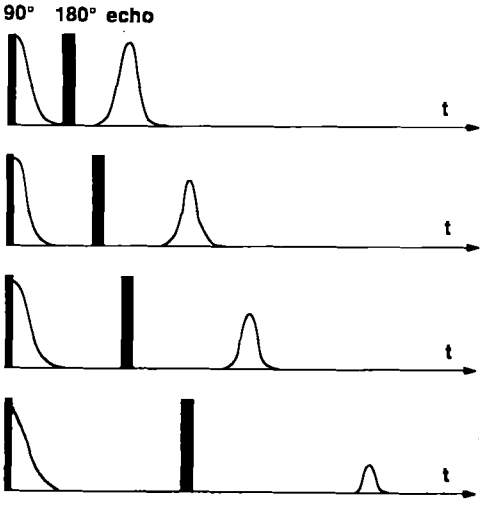


Fig. 3. NMR spin echo decay method for measuring homonuclear dipole-dipole couplings.

"spin echo" at a time $2t_1$ after the initial 90° pulse, where $t_1$ is the time delay between both pulses. Dipolar interactions among like nuclei, however, interfere with the refocusing process. Consequently the echo is diminished, depending on the length of the evolution time $2t_1$, i.e. the period over which the dipole coupling is operative.[14, 15] Very often, the echo height $I(2t_1)$ shows a Gaussian decay, whose steepness depends on the strength of the homonuclear interaction characterized by the second moment $M_{2h}$:

$$I(2t_1)/I(0) = \exp[-(2t_1)^2 M_{2h}/2] \quad (2)$$

Since most of the other solid state interactions are refocused by the above sequence, the measurement of the echo height under systematic incrementation of the evolution time $2t_1$ often affords a selective measurement of $M_{2h}$ from the semi-logarithmic plot defined by Equation 2.

### 2.4. Correlation of NMR Parameters with Structural Information

Once the correct spectroscopic parameters have been extracted, the information needs to be related to concrete structural information. Important information is often already obtained from a detailed inspection of the compositional dependence of the spectra. Furthermore, the use of crystallographically well defined reference compounds is indispensible. These methodologically simple approaches are often combined with spectroscopic simulations based on computer-modeled trial structures. Of the various interactions summarized above, only the dipolar coupling is calculable from first principles. In contrast, the interpretation of chemical shifts and quadrupolar coupling constants requires the use of semi-empirical correlations. Furthermore, the specific information that can be obtained depends highly on the certain "personality" of the nucleus under study. Table 2 gives a summary of the basic properties of nuclei typically part of chalcogenide glasses. We will limit our discussion to $^{11}B$, $^{29}Si$, and $^{31}P$, the prototype constituents of the glasses reviewed here.

**$^{11}B$.** $^{11}B$ NMR data in glasses show discrete sites $B_3$ and $B_4$, with triangular and tetrahedral coordination symmetries, respectively. These sites are separated by ca. 20 ppm in high-field $^{11}B$ MAS-NMR spectra,[20] and quantitative integration of the spectra yields $N_4$, the fraction of four-coordinate boron atoms:

$$N_4 = [B_4]/([B_4] + [B_3]) \quad (3)$$

A spectral separation can also be accomplished from traditional low-field NMR spectra on the basis of nuclear electric quadrupolar interactions.[12]

**$^{29}Si$.** $^{29}Si$ NMR data in glasses are usually interpreted in terms of various types of $SiO_4$ coordination polyhedra differing in the number of bridging Si–O–Si units. This is expressed by the $Q^{(n)}$ nomenclature, where $n$ specifies the number of such bridges per silicon present. A large number of studies have been devoted to obtaining detailed quantitative information about the $Q^{(n)}$ speciation from MAS NMR data in crystalline silicates and silicate glasses.[21] Specifically, the NMR results on alkali-metal silicate glasses are in good agreement with the traditional network modification model, in which one mole of alkali-metal oxide generates two non-bridging oxygen atoms (see Figure 4).

Table 2. Nuclear properties of magnetic isotopes present in chalcogenide glasses.

| nucleus | spin | natl. abund. [%] | resonance frequency at 7.05 T | comments on suitability for structural analysis in chalcogenide glasses |
|---|---|---|---|---|
| $^{7}Li$ | 3/2 | 92.58 | 116.59 | sensitive, but limited range of $\delta$ |
| $^{6}Li$ | 1 | 7.42 | 44.15 | limited range of $\delta$, superior in resolution to $^{7}Li$ |
| $^{11}B$ | 3/2 | 80.42 | 96.25 | sensitive, limited range of $\delta$, MAS complicated by quadrupole effects |
| $^{23}Na$ | 3/2 | 100 | 79.35 | sensitive, limited range of $\delta$, MAS complicated by quadrupole effects |
| $^{27}Al$ | 5/2 | 100 | 78.17 | sensitive, MAS complicated by quadrupole effects |
| $^{29}Si$ | 1/2 | 4.70 | 59.70 | very long relaxation times (~ 1 h) wide range of $\delta$ small chemical shift anisotropies. |
| $^{31}P$ | 1/2 | 100 | 121.44 | very sensitive, wide range of $\delta$, large chemical shift anisotropies moderately long relaxation times |
| $^{33}S$ | 3/2 | 0.76 | 23.01 | difficult to detect |
| $^{73}Ge$ | 9/2 | 7.76 | 10.47 | large quadrupole moment, |
| $^{75}As$ | 3/2 | 100 | 51.38 | poor resolution. |
| $^{77}Se$ | 1/2 | 7.58 | 57.20 | difficult to detect, wide $\delta$-range, |
| $^{125}Te$ | 1/2 | 7.00 | 94.79 | extremely large chemical shift anisotropy, long relaxation times |
| $^{205}Tl$ | 1/2 | 70.50 | 173.12 | very sensitive, wide $\delta$ range, extremely broad lines, difficult to detect with high-field instruments |

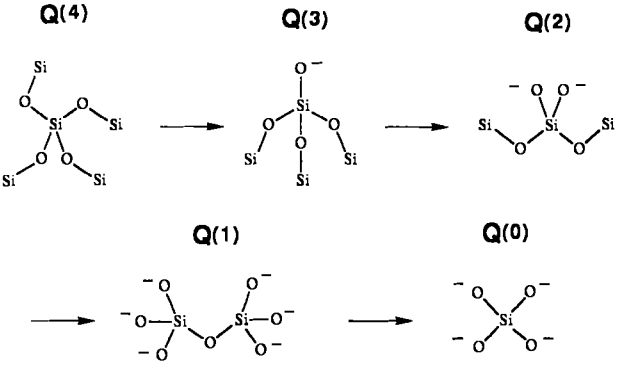


Fig. 4. Structural modification of silica glass by alkali-metal oxide modifiers, giving rise to the various $Q^{(n)}$ species. The arrow indicates increasing concentration of the modifier oxide.

ADVANCED MATERIALS

**$^{31}$P.** $^{31}$P MAS-NMR has been used in a similar fashion to provide $Q^{(n)}$ speciation in a variety of phosphates and phosphate glasses.[22] In addition valuable information is available from the measurement of the internuclear $^{31}$P–$^{31}$P interactions. Under rigid lattice conditions, $M_{2h}$ ($^{31}$P) can be calculated from van Vleck theory:[19]

$$M_{2d} = 4/15\ (\mu_0/4\pi)^2\ I\ (I+1)\ \gamma^4\ \hbar^2\ N^{-1} \sum_{i \neq j} r_{ij}^{-6} \qquad (4)$$

where $\gamma_I$, $I$, $N$, and $r_{ij}$ represent the $^{31}$P gyromagnetic ratio, the spin quantum number (½), the number of nuclei involved, and the distances between them respectively. Equation 4 permits a direct calculation of an $M_2$ value from an assumed structure. The selective measurement of internuclear $^{31}$P–$^{31}$P interactions affords a powerful tool for testing atomic distribution models in chalcogenide glasses.

## 3. Chalcogenide Glasses

### 3.1. Boron Based Glasses

Solid state NMR has been instrumental in the investigation of compound and glass formation in the systems B–S, B–Se, and B–S–Se.[23, 24] Specifically, NMR confirms that the structure of glassy $B_2S_3$ is based on the triangular $BS_{3/2}$ unit. In contrast, no such unit can be identified in corresponding B–Se glasses.[24] The composition "$B_2Se_3$" disproportionates into $BSe_2$ and an amorphous yellowish selenide $B_xSe$, which, according to the strong internuclear dipole couplings detected by NMR, must contain boron–boron bonds. This reflects the increasingly efficient competition of homoatomic (B–B and Se–Se) versus heteroatomic (B–Se) bond formation as the size of the chalcogen atom is increased.

Glassy $B_2S_3$ has a more uniform structure than glassy $B_2O_3$.[24] Nevertheless, the structural modification of $B_2S_3$ by $Li_2S$[25, 26] and $Tl_2S$[27] is an excellent analogy to the well-studied behavior of borate glasses.[12] Glasses in the systems $(Li_2S)_x(B_2S_3)_{1-x}$ and $(Tl_2S)_x(B_2S_3)_{1-x}$ are formed for $0 \leq x \leq 0.75$, with phase separation occurring at low x-values. In both cases, small amounts of $Li_2S$ and $Tl_2S$ cause a network transformation resulting in the production of four-coordinate boron atoms. Above a ratio $Li_2S(Tl_2S)/B_2S_3$ of 0.5, the number of four-coordinate boron atoms decreases again, because units containing non-bridging sulfur atoms are formed in this regime. This compositional dependence of $N_4$ is in good agreement with the respective oxygen-based systems.[12, 28]

### 3.2. Silicon Based Glasses

Besides offering promise for applications in infrared optics and semiconductor technology, silicon chalcogenide glasses are of fundamental interest in glass science. Vibrational spectroscopic data suggest that the structure of these glasses contains linear chain polymers composed of edge-sharing $SiSe_{4/2}$ units.[29] This finding is a striking exception from the general rule that glasses organize exclusively by corner-sharing of coordination polyhedra.

Figure 5 shows typical $^{29}$Si MAS-NMR spectra in the system silicon–selenium.[30] Note that multiple sites are present, even in the stoichiometric glass of composition $SiSe_2$. The spectra show three distinct resonances which are assigned to Si atoms involved in zero, one and two edge-sharing tetrahedra, labeled $E^{(0)}$, $E^{(1)}$, and $E^{(2)}$ in Figure 5.[31] Increasing the selenium content in the glasses favors corner sharing. The evaluation of these units is made difficult by the extremely long $T_1$ values in these glasses.[30, 31] Absolute signal intensity calibrations with standards containing known amounts of silicon show that with 90° pulses and recycle delays of 2 h, 85–95% of the total Si atoms are detected in these systems.[30] This control experiment ensures that the speciation inferred from NMR is truly representative of the entire glass.

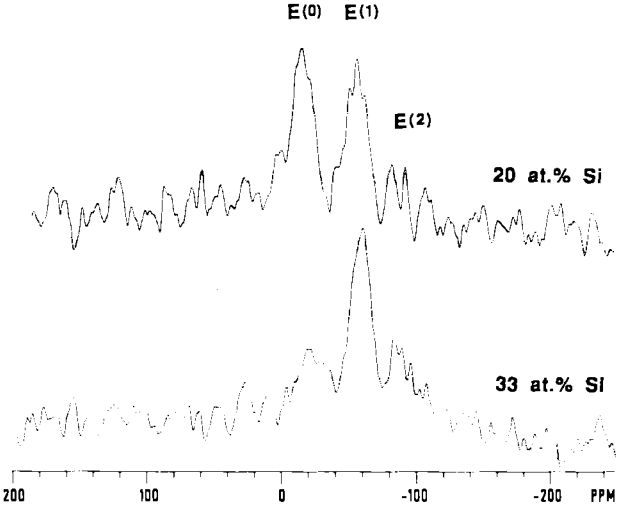


Fig. 5. $^{29}$Si MAS-NMR spectra of glasses in the system Si–Se. The resonances are assigned to (from left to right in order of increasing field): corner-sharing $SiSe_{4/2}$ tetrahedra ($E^{(0)}$), $SiSe_{4/2}$ groups involved in one edge-sharing tetrahedron ($E^{(1)}$), and $SiSe_{4/2}$ groups involved in two edge-sharing tetrahedra ($E^{(2)}$), respectively. Note the compositional dependence. The poor signal-to-noise ratio arises from the extremely long spin-lattice relaxation times in these samples, requiring recycle delays of 2 h.

Lithium silicon sulfide glasses show promise for solid electrolyte applications.[32] The region of glass-formation of the system $(Li_2S)_x$-$(SiS_2)_{1-x}$ ranges from $x = 0$ to $x = 0.6$ (glasses formed in the compositional region $0 < x < 0.4$ may be phase separated). Given the unusual structural properties of the parent $SiS_2$ and $SiSe_2$ glasses, new types of microstructures might be expected in the glasses modified analogously by alkali metal sulfides. A detailed $^{29}$Si MAS NMR study of the system $Li_2S$-$SiS_2$ was undertaken to test whether the $Q^{(n)}$

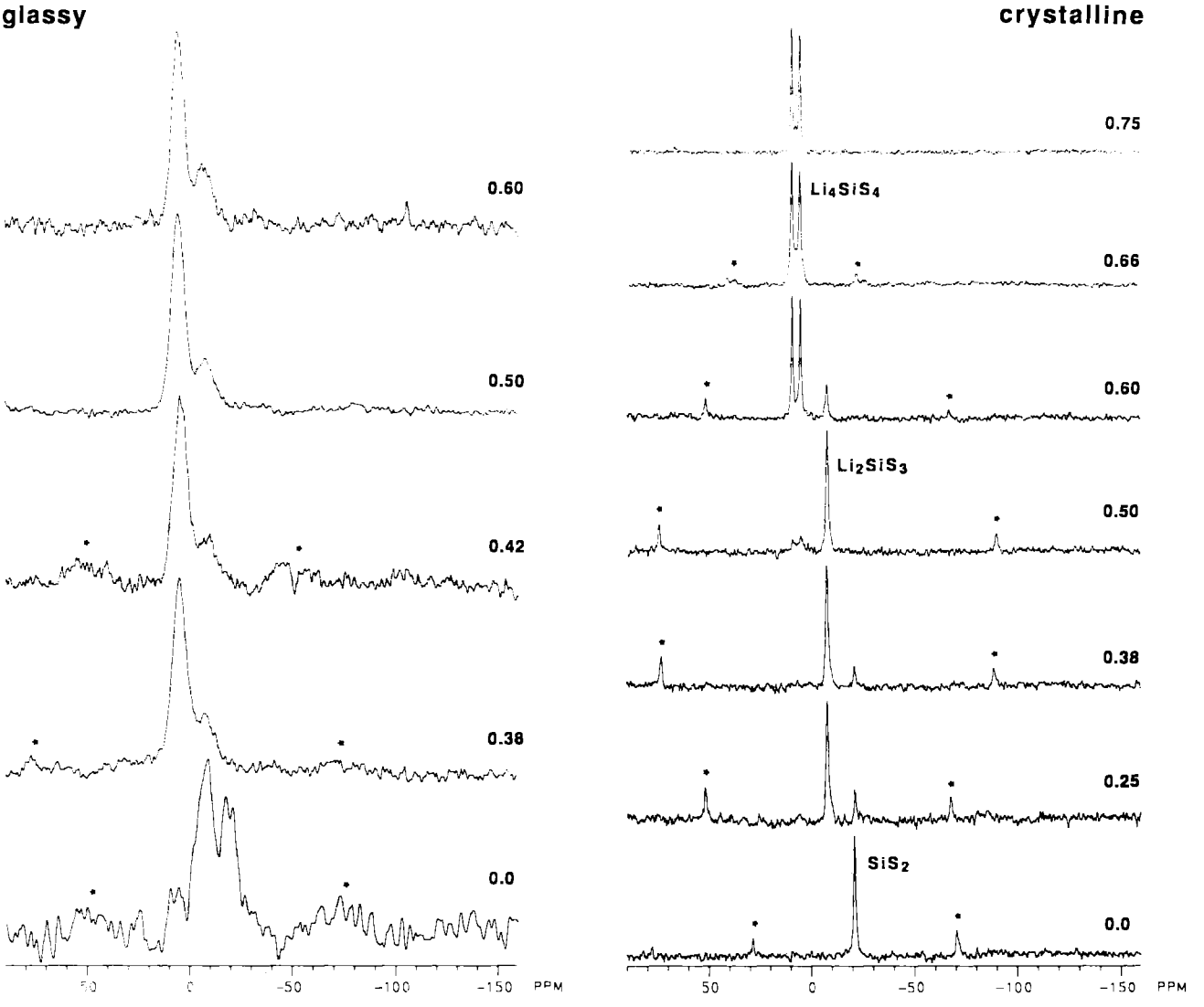


Fig. 6. 59.9 MHz $^{29}Si$ MAS-NMR spectra of glassy and crystalline samples in the system $(Li_2S)_x(SiS_2)_{1-x}$. For $x \geq 0.4$, the spectra show no obvious chemical shift evolution in the glasses, in contrast to the situation in the crystalline phases.

concept valid in the oxidic glasses (Figure 4) is also applicable to sulfide-based glasses.[33] The results are shown in Figure 6. Virtually no compositional evolution can be detected in the ternary glasses, whereas the corresponding crystallized specimens reveal marked changes. These findings were initially interpreted in terms of a constant number of non-bridging sulfur atoms regardless of $Li_2S$ content. The two resonances were assigned to $Q^{(0)}$ species (major resonance around 4–8 ppm) and $Q^{(2)}$ species (minor peak around $-6$ to $-10$ ppm), based on previous assumptions in the literature[34] that the structures of $Li_4SiS_4$ and $Li_2SiS_3$ contain corner shared $Q^{(0)}$ and $Q^{(2)}$ environments (no single crystal X-ray work has been carried out). The original interpretation dismisses the traditional model of continous network modification and invokes a number of non-bridging sulfur atoms that is much larger than expected from the $Li_2S$ content.

Subsequent work on a larger number of better characterized crystalline alkali thiosilicates[35] suggests that the chemical shift discrimination seen in the spectra of Figure 6a is most likely not due to the various $Q^{(n)}$ species but due to the number of edge sharing tetrahedra, $E^{(n)}$, in which the Si atom under consideration is involved.[36] According to this reinterpretation, the majority peak around 4–8 ppm arises from Si atoms involved exclusively in corner sharing with other tetrahedra ($E^{(0)}$), while the minority peak around $-6$ to $-10$ ppm is assigned to units engaging in edge-sharing with one other $SiS_4$ tetrahedron ($E^{(1)}$). Based on these assignments, the spectra reveal that $Li_2S$ decreases the amount of edge-sharing dramatically, such that no $E^{(2)}$ units remain at 38 mole-% $Li_2S$ or above. The work on the crystalline model compounds suggests further, that the chemical shift differences between Si atoms containing different numbers of non-bridging S atoms (i.e. the sulfide-analogs of the various $Q^{(n)}$

ADVANCED MATERIALS

species of Figure 4) are much smaller in sulfides than in oxides. Given the inherently broad MAS-NMR lines in the glasses, it is not possible to resolve individual peaks for these species. Therefore, there is no proof from NMR that the $Q^{(n)}$ concept is actually valid in sulfide glasses. If, however, the assumption is made as a working hypothesis, one arrives at the peak assignments summarized in Figure 7 in the form of

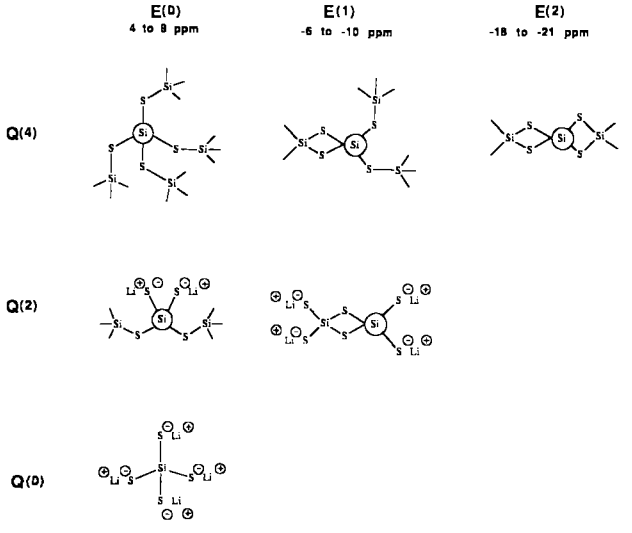


Fig. 7. Suggested peak assignments in the system $Li_2S$–$SiS_2$.

a matrix. Each microstructure can be represented by a $Q^{(n)}$ *and* an $E^{(n)}$ symbol. The NMR spectra then show that, at low $Li_2S$ contents, the production of non-bridging sulfur atoms preferably occurs at the $E^{(1)}$ and $E^{(2)}$ sites. The constant ratio of $E^{(0)}$ to $E^{(1)}$ units at higher $Li_2S$ contents suggests that some balance has been attained between the destruction of edge- and corner-sharing Si–S–Si units.

### 3.3. Phosphorus Based Glasses

Both the binary systems P–S and P–Se are well known to form stable glasses, with P concentrations ranging from 0–25 at.-% P in the former, and 0–52 as well as 62–80 at.-%.P in the latter system.[37–41] Phosphorus–Selenium glasses are of particular interest because of their infrared-transparency, their comparatively high stability in a moist atmosphere, and their resistance towards recrystallization. The microscopic structure of these glasses has been the subject of an interesting controversy. On the one hand, *Borisova* et al.[37] as well as *Blachnik* and coworkers[38] propose what basically amounts to a chemically ordered continuous random network model: at P contents below 40 at.-% the glasses contain $Se=PSe_{3/2}$, $PSe_{3/2}$ and Se–Se units only, whereas no P–P bonds exist. Above 40 at.-% P, these authors suggest an abrupt increase in the fraction of P–P bonds, hence rationalizing the steep increase of glass transition temperatures which is experimentally observed in this compositional region.

In sharp contrast, combined EXAFS and neutron diffraction studies point toward an entirely different glass structure based on $P_4Se_n$ clusters ($5 \geq n \geq 3$, depending on the P/Se ratio) which are embedded in an Se-rich matrix.[42] Such an arrangement constitutes substantial intermediate range order, as has been recently suggested for other glass systems.

The two conflicting models differ largely with respect to the distribution of the P atoms in space. Figure 8 shows three

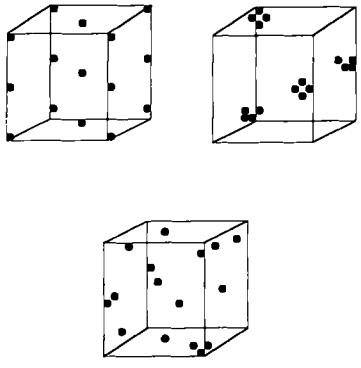

Fig. 8. Simple atomic distribution models for P atoms in P–Se glasses, corresponding to uniform, clustered, and random arrangements.

simplistic atomic distribution models for P–Se glasses, corresponding to a) a uniform, b) a clustered and c) a random distribution of P atoms. These arrangements are clearly distinguishable by the magnitude and the compositional dependence of the dipole-dipole couplings between the $^{31}P$ nuclear spins. Thus, using the spin-echo sequence discussed in Section 2, the second moments characterizing these internuclear

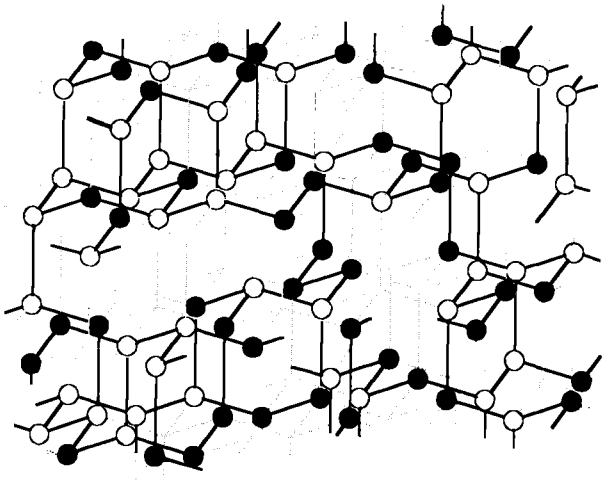

Fig. 9. Graphical illustration of the randomly occupied zinc blende structure used as a model for a P–Se glass containing 50 at.-% P. Open circles denote P atoms, filled circles Se atoms. The dotted lines represent non-bonding electron pairs pointing towards a vacancy in the structure.

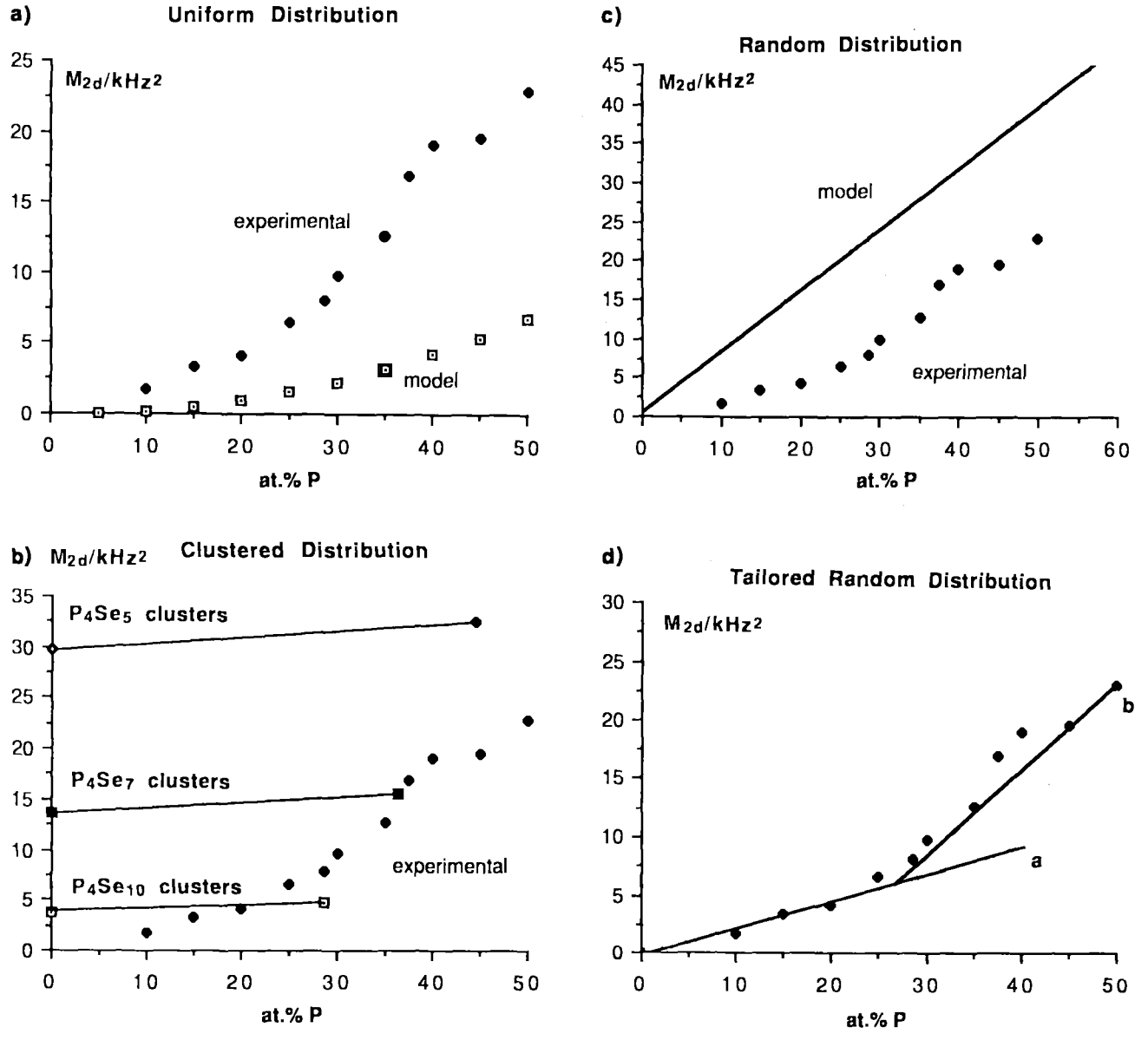


Fig. 10. Comparison of the compositional dependence of the $^{31}P$ dipolar second moment characterizing the strength of homonuclear $^{31}P$–$^{31}P$ dipolar interactions with calculations based on assumed atomic distribution models in P–Se glasses. See text for further discussion. The tailored random distribution assumes that no P–P bonds are present below 25 at.-% P (line a) and a probability of (X-25%) at all compositions with higher P contents X at.-% (line b).

interactions can be measured and compared with calculated values (using Equation 4) based on various assumed distribution models.

In order to simulate a random distribution, the P and Se atoms are positioned irregularly, according to their atomic percentages, over the sites of a cubic zinc blende structure. The chosen lattice constant (5.289 Å) constrains the nearest neighbor distance to 2.29 Å, corresponding to the average of typical P–P, P–Se, and Se–Se bond lengths. Furthermore, the random model incorporates the valency constraints of P and Se by distributing nonbonding electron pairs over additional lattice positions. Figure 9 shows an example of a random distribution generated in this way. This model reproduces the experimental densities of the glasses quite well (within 5–10%).

The comparison between calculated and experimental $M_2$ values is shown in Figure 10. Clearly, the experimental data are incompatible with either uniform, clustered or random distribution models. If however, the random model is adapted in terms of a reduced probability of P–P bonds, an excellent fit to the experimental data can be obtained. The comparison of Figure 10c with 10d indicates that, at any composition within the glass forming region, there is a distinct preference for P–Se over P–P bonds. Overall, the NMR results can be understood in terms of a random distribution of P and Se atoms over a glass structure, modeled as a defect

ADVANCED MATERIALS

zinc blende lattice, excluding P–P bonds below 25 at.-% P and admitting them in less than statistical proportions above 25 at.-%.[43,44]

While such dipolar measurements provide important insights concerning the statistics of P–P versus P–Se bonding in these glasses, they are unable to identify the distinct nearest neighbor environments present. Such information can be provided by MAS-NMR in conjunction with data obtained on crystalline reference compounds.[44–46] Figure 11 shows typical results in the P–Se system.[45] At P contents below 30 at.-%, two well-resolved peaks are observed which

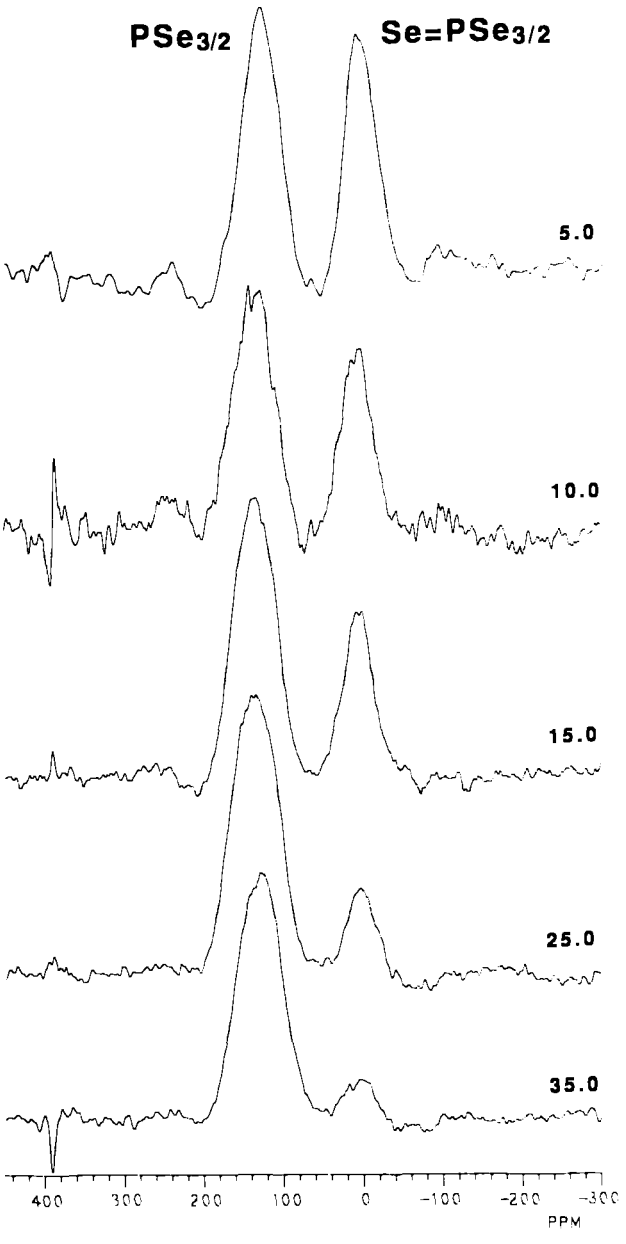


Fig. 11. 121.5 MHz $^{31}$P MAS-NMR spectra of P–Se glasses. Numerals indicate at.-% phosphorus. The two resonances are assigned to three-coordinated ($PSe_{3/2}$ and $Se_{2/2}P–PSe_{2/2}$, downfield resonance, left) and four coordinated $Se=PSe_{3/2}$ species (upfield resonance, right), respectively.

are assigned to three-coordinated $PSe_{3/2}$ and tetrahedral $Se=PSe_{3/2}$ groups, respectively.

Quantitative integration of these spectra yields a phenomenological equilibrium constant K of 0.85 (at.-fraction)$^{-1}$ associated with the melt reaction $PSe_{3/2} + [Se_a]_{1/n} \rightarrow Se=PSe_{3/2}$. Figure 12 shows the experimental data for the fraction $N_4$ of

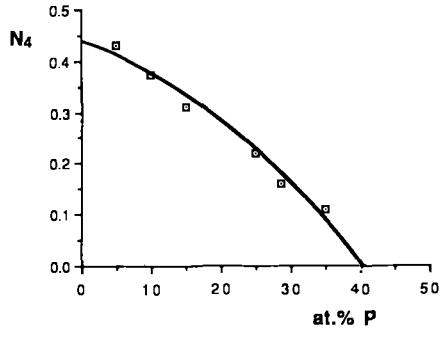


Fig. 12. Dependence of the fraction of four-coordinated $Se=PSe_{3/2}$ units, $N_4$, (open squares) on the atomic fraction of P atoms in P–Se glasses. The solid curve is calculated based on an equilibrium constant K = 0.85 (at.-fraction)$^{-1}$ of the reaction $PSe_{3/2} + Se \rightarrow Se=PSe_{3/2}$.

the four-coordinate P atoms as a function of composition and the corresponding theoretical fit. The near-unity value of K reflects the efficient competition of the three entities that take part in the above reaction, hence providing a thermodynamic rationale for the excessive tendency of glass-formation in this system.

It is interesting to compare these results with corresponding data obtained on the system P–S.[47] According to $^{31}$P MAS and spin echo NMR data, the $S=PS_{3/2}$ grouping is the dominant structural unit within the entire glass forming region. This leads to crystallization of $P_4S_9$ and $P_4S_{10}$ above 25 at.-% P. In fact, MAS-NMR studies of P–S glasses detect molecular $P_4S_9$ and $P_4S_{10}$ entities well below the compositional glass-forming border. Likewise, NMR detects $P_4Se_3$ molecules in P–Se glasses with P contents well below the stoichiometry of this compound.[45] The presence of such molecular entities near and somewhat below the glass-forming border appears to be a general feature of glass formation in phosphorus chalcogenide systems.

## 4. Summary and Outlook

The experimental results covered in this review show that the degree to which the structural principles operative in non-oxide chalcogenide glasses differ from the bonding concepts used in the stoichiometrically analogous oxidic glasses depend greatly on the system under study. Specifically, in boron chalcogenide-based systems, there seems to be very close similarity between oxides and sulfides. In contrast, the edge-shared micro-environments identified in $SiS_2$, Si–Se,

and $Li_2S$ $SiS_2$ glasses are fundamentally new structures not known to exist in ordinary silica-based glasses. The latter statement also holds true for phosphorus chalcogenide glasses. Specifically in the P–Se glasses, there is a multitude of micro-environments, containing three- and four coordinate P atoms as well as various P–P bonded structures and, near the glassforming border, molecular cluster units.

The attractiveness of NMR spectroscopy for these systems lies in the opportunity of providing actual percentages with which these structural features occur, provided the experiments are done under quantitative conditions. Due to their element-selectivity, NMR methods have a decisive advantage over other competing structural probes for the compositionally more complex systems usually encountered in "real-life" practical applications. This advantage has already been exploited in our NMR studies of the co-former effect in $Li_2S$–$B_2S_3$–$P_2S_5$ and $Li_2S$–$SiS_2$–$P_2S_5$ glasses.[25,48] The studies reported here have laid the groundwork for such further investigations and the author hopes that this review will help to popularize the use of quantitative solid state NMR techniques in the structural elucidation of chalcogenide glasses.

Received: July 17, 1989

[1] P. C. Taylor, *Mater. Res. Soc. Bull. 1987*, p. 36. A. M. Andriesh, *J. Non-Cryst. Solids 77/78* (1985) 1219. A. R. Hilton, C. E. Jones, M. J. Brau, *Infrared Phys. 4* (1964) 213.
[2] S. R. Ovshinsky, *Phys. Rev. Lett. 21* (1968) 1450.
[3] M. Kastner, *J. Non-Cryst. Solids 35–36* (1980) 807. D. Adler, *J. Non-Cryst. Solids 73*, (1985) 205, and references therein.
[4] R. G. Brandes, F. P. Laming, A. D. Pearson, *Appl. Opt. 9* (1970) 1712.
[5] S. Sahami, S. W. Shea, J. H. Kennedy, *J. Electrochem. Soc. 132* (1985) 985. J. H. Kennedy, S. Sahami, S. W. Shea, Z. Zhang, *Solid State Ionics 18/19* (1986) 368.
[6] For early seminal work on glass formation in chalcogenide systems, see A. R. Hilton, C. E. Jones, M. Brau, *Phys. Chem. Glasses 7* (1966) 105. B. T. Kolomiets, *Phys. Status Solidi 7* (1964) 359, 713. See also: Z. U. Borisova: *Glassy Semiconductors*, Plenum Press, New York 1981, and references therein.
[7] S. A. Dembovskii, E. A. Chechetkina, *J. Non-Cryst. Solids 85* (1986) 364. J. Bicerano, S. R. Ovshinsky, *J. Non-Cryst. Solids 74* (1985) 75.
[8] M. Tenhover, M. A. Hazle, R. K. Grasselli, *Phys. Rev. B29* (1984) 6732. R. W. Johnson, D. L. Price, S. Susman, M. Arai, T. I. Morrison, G. K. Shenoy, *J. Non-Cryst. Solids 83* (1986) 251.
[9] P. Boolchand, *Hyperfine Interact. 27* (1986) 3. J. C. Phillips, *J. Non-Cryst. Solids 43* (1981) 37. J. C. Phillips, *ibid 34* (1979) 153.
[10] Comprehensive discussions of the structural problem in glasses can be found in R. Zallen: *The Physics of Amorphous Solids*, Wiley, New York 1983; R. A. Weeks, *J. Non-Cryst. Solids 73* (1985) 103. For recent molecular dynamics simulations, see C. A. Angell, *J. Non-Cryst. Solids 73* (1985) 1. P. Vashishta, R. K. Kalia, I. Ebbsjö, *J. Non-Cryst. Solids 106* (1988) 301. G. A. Antonio, R. K. Kalia, P. Vashishta, *J. Non-Cryst. Solids 106* (1988) 305.
[11] For an excellent review of solid state NMR, see T. M. Duncan, C. R. Dybowski, *Surf. Sci. Rep. 1* (1981) 157. See also M. Mehring: *Principles of High Resolution NMR in Solids*, Springer, Heidelberg 1983.
[12] Comprehensive reviews of NMR applications to glasses can be found in W. Müller-Warmuth, H. Eckert, *Phys. Rep. 88* (1982) 91. P. J. Bray, *J. Non-Cryst. Solids 73* (1985) 19. G. L. Turner, R. J. Kirkpatrick, S. H. Risbud, E. Oldfield, *Am. Ceram. Soc. Bull. 66* (1987) 656.
[13] E. R. Andrew, A. Bradbury, R. G. Eades, *Nature 183* (1959) 1802. I. J. Lowe, *Phys. Rev. Lett. 2* (1959) 285.
[14] M. Engelsberg, R. E. Norberg, *Phys. Rev. B5* (1972) 3395.
[15] N. Boden, M. Gibb, Y. K. Levine, M. Mortimer, *J. Magn. Reson. 16* (1974) 471.
[16] A. P. M. Kentgens, J. J. M. Lemmens, F. M. M. Geurts, W. S. Veeman, *J. Magn. Reson. 71* (1987) 62. A. Samoson, E. Kundla, E. Lippmaa, *J. Magn. Reson. 49* (1982) 350.
[17] M. M. Maricq, J. S. Waugh, *J. Chem. Phys. 70* (1979) 3300. J. Herzfeld, A. E. Berger, *J. Chem. Phys. 73* (1980) 6021.
[18] S. Ganapathy, S. Schramm, E. Oldfield, *J. Chem. Phys. 77* (1982) 4360.
[19] J. H. Van Vleck, *Phys. Rev. 74* (1948) 1168.
[20] G. L. Turner, K. A. Smith, R. J. Kirkpatrick, E. Oldfield, *J. Magn. Reson. 67* (1986) 544.
[21] E. Lippmaa, M. Mägi, A. Samoson, G. Engelhardt, A. R. Grimmer, *J. Am. Chem. Soc. 102* (1980) 4889. K. A. Smith, R. J. Kirkpatrick, E. Oldfield, D. M. Henderson, *Am. Mineral. 68* (1983) 1206. A. R. Grimmer, M. Mägi, M. Hähnert, H. Stade, A. Samoson, W. Wieker, E. Lippmaa, *Phys. Chem. Glasses 25* (1984) 105. R. Dupree, D. Holland, P. W. McMillan, R. F. Pettifer, *J. Non-Cryst. Solids 68* (1984) 399. J. B. Murdoch, J. F. Stebbins, I. S. E. Carmichael, *Am. Mineral. 70* (1985) 332. R. J. Kirkpatrick, K. A. Smith, R. A. Kinsey, E. Oldfield, *Am. Mineral. 70* (1985) 106. E. Schneider, J. F. Stebbins, A. Pines, *J. Non-Cryst. Solids 89* (1987) 371.
[22] G. L. Turner, K. A. Smith, R. J. Kirkpatrick, E. Oldfield, *J. Magn. Reson. 70* (1986) 408. M. Villa, K. R. Carduner, G. Chiodelli, *J. Non-Cryst. Solids 94* (1987) 101.
[23] M. Rubinstein, *Phys. Rev. B14* (1976) 2778.
[24] H. U. Hürter, B. Krebs, H. Eckert, W. Müller-Warmuth, *Inorg. Chem. 24* (1985) 1288.
[25] Z. Zhang, J. H. Kennedy, J. Thompson, S. Anderson, D. A. Lathrop, H. Eckert, *Appl. Phys. A* (1989) *49* (1989) 41.
[26] D. E. Hintenlang, P. J. Bray, *J. Non-Cryst. Solids 69* (1985) 243.
[27] H. Eckert, W. Müller-Warmuth, W. Hamann, B. Krebs, *J. Non-Cryst. Solids 65* (1984) 53.
[28] J. F. Baugher, P. J. Bray, *Phys. Chem. Glasses 10* (1969) 77.
[29] M. Tenhover, R. S. Henderson, D. Lukco, M. A. Hazle, R. K. Grasselli, *Solid State Commun. 51* (1984) 455. M. Tenhover, M. A. Hazle, R. K. Grasselli, *Phys. Rev. Lett. 51* (1983) 404.
[30] K. Moran, R. Shibao, H. Eckert, unpublished.
[31] M. Tenhover, R. D. Boyer, R. S. Henderson, T. E. Hammond, G. A. Shreve, *Solid State Commun. 65* (1988) 1517.
[32] J. H. Kennedy, Z. Zhang, *J. Electrochem. Soc. 135* (1988) 859.
[33] H. Eckert, Z. Zhang, J. H. Kennedy, *J. Non-Cryst. Solids*, 107 (1989) 271.
[34] A. Haas, *Angew. Chem. Int. Ed. Engl. 4* (1965) 1014; *Angew. Chem. 77* (1965) 1066. A. Weiss, G. Rocktaeschel, *Z. Anorg. Allg. Chem. 307* (1960) 1.
[35] J. Olivier-Fourcade, J. C. Jumas, M. Ribes, E. Phillipot, M. Maurin, *J. Solid State Chem. 23* (1978) 155. B. Krebs, *Angew. Chem. Int. Ed. Engl. 22* (1983) 113; *Angew. Chem. 95* (1983) 113.
[36] H. Eckert, J. H. Kennedy, A. Pradel, M. Ribes, unpublished.
[37] Z. U. Borisova, B. E. Kasatkin, E. I. Kim, *Izv. Akad. Nauk SSSR Neorg. Mater. 9* (1973) 822.
[38] R. Blachnik, A. Hoppe, *J. Non-Cryst. Solids 34* (1979) 191.
[39] F. Heyder, D. Linke, *Z. Chem. 13* (1973) 480.
[40] Y. Monteil, H. Vincent, *J. Inorg. Nucl. Chem. 37* (1975) 2053.
[41] Y. Monteil, H. Vincent, *Z. Anorg. Allg. Chem. 416* (1975) 181.
[42] D. L. Price, M. Misawa, S. Susman, T. I. Morrison, G. K. Shenoy, M. Grimsditch, *J. Non-Cryst. Solids 66* (1984) 443. M. Arai, R. W. Johnson, D. L. Price, S. Susman, M. Gay, J. E. Enderby, *J. Non-Cryst. Solids 83* (1986) 80.
[43] D. Lathrop, H. Eckert, *J. Am. Chem. Soc. 111* (1989) 3536.
[44] D. Lathrop, H. Eckert, *J. Non-Cryst. Solids 106* (1988) 417.
[45] D. Lathrop, H. Eckert, *J. Phys. Chem.* in press.
[46] H. Eckert, C. S. Liang, G. D. Stucky, *J. Phys. Chem. 93* (1989) 452.
[47] M. Tullius, D. Lathrop, H. Eckert, *J. Phys. Chem.* in press.
[48] H. Eckert, Z. Zhang, J. H. Kennedy, *Mater. Res. Soc. Symp. Proc. 135* (1989) 259.